THE JOURNAL OF PHYSICAL CHEMISTRY B

pubs.acs.org/JPCB

Article

Protein Side-Chain–DNA Contacts Probed by Fast Magic-Angle Spinning NMR

Published as part of The Journal of Physical Chemistry virtual special issue "Hellmut Eckert Festschrift".

Denis Lacabanne, Julien Boudet, Alexander A. Malär, Pengzhi Wu, Riccardo Cadalbert, Loic Salmon, Frédéric H.-T. Allain,* Beat H. Meier,* and Thomas Wiegand*

Cite This: *J. Phys. Chem. B* 2020, 124, 11089–11097

Read Online

ACCESS | Metrics & More | Article Recommendations | Supporting Information

ABSTRACT: Protein–nucleic acid interactions are essential in a variety of biological events ranging from the replication of genomic DNA to the synthesis of proteins. Noncovalent interactions guide such molecular recognition events, and protons are often at the center of them, particularly due to their capability of forming hydrogen bonds to the nucleic acid phosphate groups. Fast magic-angle spinning experiments (100 kHz) reduce the proton NMR line width in solid-state NMR of fully protonated protein–DNA complexes to such an extent that resolved proton signals from side-chains coordinating the DNA can be detected. We describe a set of NMR experiments focusing on the detection of protein side-chains from lysine, arginine, and aromatic amino acids and discuss the conclusions that can be obtained on their role in DNA coordination. We studied the 39 kDa enzyme of the archaeal pRN1 primase complexed with DNA and characterize protein–DNA contacts in the presence and absence of bound ATP molecules.

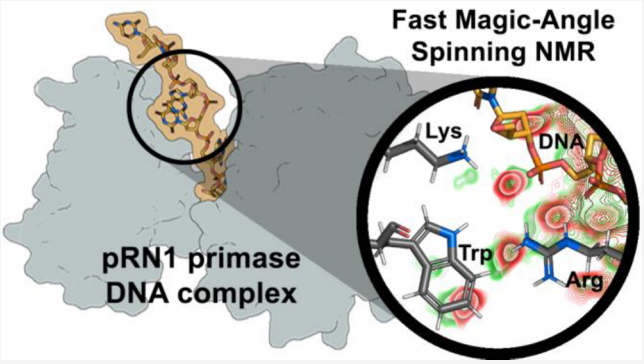

INTRODUCTION

Protein–nucleic acid interactions are essential in many biological processes, such as DNA replication, DNA transcription, and DNA repair. The underlying molecular recognition processes are directed by noncovalent interactions, among them hydrogen bonds (including also water-mediated hydrogen bonds), electrostatic Coulomb interactions, and van-der-Waals contacts.[1−4] Up to now, protein–nucleic acid contacts have been mainly probed structurally at the atomic level by X-ray crystallography[2,5,6] and cryo-electron microscopy (cyro-EM).[7−10] X-ray crystallography requires suitable single crystals of the protein–DNA complexes, while for EM, the protein complexes have to orient randomly on the EM grid.[11−13] In cases where crystallization fails or the resolution of the obtained structures is not sufficient to clearly identify protein–DNA interactions, NMR in solution[14,15] or in the solid state[16−22] is an attractive option. Indeed, the NMR chemical shift is highly sensitive to protein–DNA interactions. Less shielded ^{1}H resonances indicate a participation of the proton in a hydrogen bond.[23,24] Changes in dynamics of protein side-chains (as well as backbone) upon DNA binding[25] (e.g., salt-bridge formation involving lysine side-chains) can be reflected in intensity changes or by appearing or disappearing peaks in NMR spectra.[26,27]

Solution-state NMR has explored intensively noncovalent protein–nucleic acid interactions[14,28] and allows the characterization of small to medium size protein–nucleic acid complexes (~15 to 60 kDa). In order to obtain high-resolution spectra for large proteins, TROSY (transverse relaxation-optimized spectroscopy) experiments are required[29,30] making proteins of 500 kDa to 1 MDa accessible for NMR.[31,32] In contrast, solid-state NMR studies, using the detection of protons as probes for protein–DNA interactions, are still rare[16,24] as technical challenges limited the detection of high-resolution solid-state proton spectra. However, MAS experiments at spinning frequencies above 100 kHz were implemented in previous years leading to good spectral resolution even for fully protonated proteins[33−44] and nucleic acids.[45] Solid-state NMR benefits from straightforward sample preparation, since the protein–nucleic acid complexes are sedimented directly in the MAS rotor[46−48] avoiding a crystallization step which often fails for these assemblies, e.g. due to residual flexibility of bound

Received: September 7, 2020
Revised: November 15, 2020
Published: November 26, 2020

https://dx.doi.org/10.1021/acs.jpcb.0c08150
J. Phys. Chem. B 2020, 124, 11089–11097

nucleic acids[49] or as a consequence of the transient nature of such interactions.[50] In many cases, long-term stable protein sediments are obtained in which even the hydrolysis of ATP is significantly reduced.[48] For MAS experiments above 100 kHz, 300 μg of sample is required which is typically significantly less than needed for a solution-state NMR experiment. In solids, no protein-size dependent line broadening exists and special isotope labeling schemes[30] or segmental labeling approaches[51−53] can be used in order to decongest the spectra thus resolving assignment ambiguities.[30]

We describe in this work solid-state NMR experiments which detect protein−DNA contacts in the archaeal pRN1 primase from *Sulfolobus islandicus*[54] by detecting protein resonances. The DNA remains in natural abundance in our studies. Primases in the context of DNA replication synthesize a short oligonucleotide (primer) and are crucial to initiate the DNA polymerization *de novo*.[55] The pRN1 primase (protein with around 900 residues) is composed of a catalytic N-terminal Prim_Pol domain (residues 47−247), a helix bundle domain (HBD, residues 256−370), a helicase domain (residues 408−827), and a C-terminal winged helix DNA-binding domain (residues 752−844).[56,57] Since the pRN1 primase function is efficiently and exclusively preserved with the helix bundle and the Prim_Pol domains,[56] we investigate a construct comprising both of them (residues 40−370, 39 kDa, denoted in the following as pRN1).[56,58] Functionally, the HBD serves as a platform for binding the crucial GTG motif providing the template for the polymerization site located in the Prim_Pol domain.[59] The DNA sequence-specificity of the HBD is significantly enhanced by major conformational changes upon binding to two ATP nucleotides suggesting that the HBD brings the substrates together for initiating the primer synthesis.[58] In recent work, we have illustrated that solid-state NMR restraints added in the solution-state NMR structure calculation of the HBD complexed with two ATP molecules and a DNA strand (in the following denoted as pRN1:ATP:DNA) resolve intermolecular restraint ambiguities and improve the precision of the structure calculation, especially for the location of the ATP triphosphate groups.[58]

Here we report the solid-state NMR experiments probing key protein−DNA contacts on the fully protonated pRN1 primase. Figure 1 summarizes the experimental approach and the nuclei observed. Our protocol is based on (i) detecting bound and thus immobilized ATP and DNA molecules by ^{31}P-detection, (ii) probing spatial protein−DNA correlations by ^{31}P-detected heteronuclear correlation experiments (such as NHHP and CHHP where the ^{13}C and ^{15}N spins are localized on the protein;[20,24] this type of experiment benefits from easy-to-optimize ^{1}H,^{13}C/^{15}N, and ^{1}H,^{31}P cross-polarization transfer steps which are important if the experimental signal-to-noise ratio is limited), (iii) identifying, in hNH spectra, arginine side-chain NH proton resonances that coordinate to nucleotides by the typical deshielding indicating that the proton contributes to a hydrogen bond, (iv) identifying lysine side-chains forming salt bridges to the DNA phosphate backbone, and (v) identifying aromatic side-chains in ^{1}H-detected spectra. In this work, we show structural insights into DNA binding to the pRN1 enzyme gained from points (iii)−(v) (^{31}P-detected experiments were described in a previous work[58]) paving the way for an atomic scale model of its conformational activation.

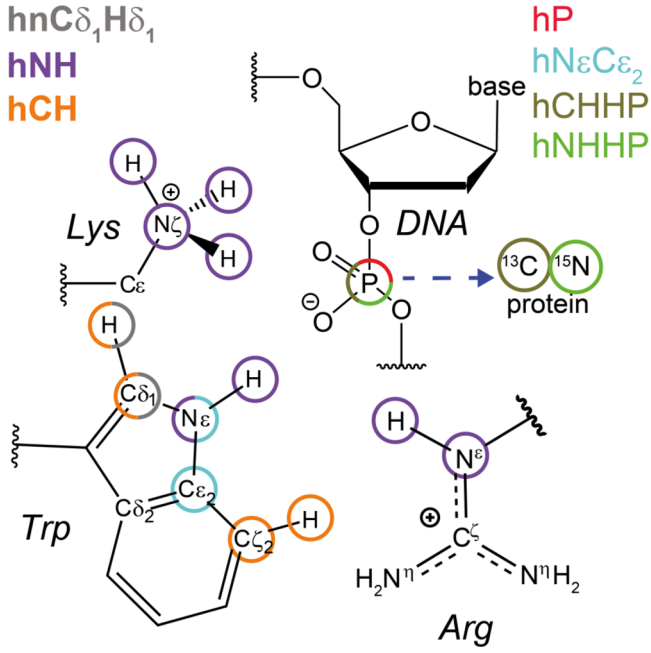

Figure 1. Solid-state NMR experiments to probe protein−nucleic acid interactions. Representation of correlations observed in a combination of solid-state NMR experiments to detect protein−nucleic acid contacts. Lysine, arginine, and tryptophan side-chains are shown as illustrative residues coordinating to a DNA strand. In this work, hn$C\delta_1H\delta_1$, hNH, hCH, and hN$\varepsilon C\varepsilon_2$ were used.

RESULTS AND DISCUSSION

Proton-Detected Solid-State NMR: Sequential Resonance Assignment. ^{31}P-detected CHHP and NHHP experiments reveal spatial proximities between the protein and DNA phosphate groups as discussed previously[58] for pRN1. In contrast, ^{1}H chemical-shift values are very sensitive to noncovalent interactions and represent powerful probes for interactions between side-chain protons and nucleotides. Figure 2A shows the solid-state ^{1}H,^{15}N cross-polarization (CP)-based hNH spectrum of the fully protonated pRN1:ATP:DNA complex (colored in light green, for an overlay of the spectra of pRN1:DNA and pRN1:ATP:DNA, see Figure S1) recorded at 100 kHz MAS. The average ^{1}H line width (full-width at half-maximum, fwhm) for the 18 isolated peaks marked by crosses in Figure S1 is determined to be 180 ± 30 Hz which is in the typical-range for fully protonated proteins at 100 kHz MAS.[24,40,60,61] Those fwhm are still dominated by homogeneous line broadening mechanisms which could potentially be further scaled down by faster MAS experiments.[60,62,63]

The observed line widths allow for a sequential resonance assignment using multidimensional NMR experiments, although most assignments can be transferred from solution to the solid state in the present case (*vide infra*). Two-dimensional planes of 3D hCANH and hNCAH spectra for the pRN1:ATP:DNA complex are reported in Figure 2A. We have applied an assignment strategy relying on amide $^{1}H^{N}$ and aliphatic $^{1}H^{A}$ protons in four 3D spectra: two intraresidual spectra (hCANH and hNCAH) are combined with two interresidual experiments (hNcoCAH and hCAcoNH).[24] Our assignment was performed using this set of 3D data and cross-checked by the solution-state chemical shifts for the HBD and Prim_Pol domain (BMRB accession code 34290). In some cases, assignments obtained in solution were transferred to the

https://dx.doi.org/10.1021/acs.jpcb.0c08150
J. Phys. Chem. B 2020, 124, 11089−11097

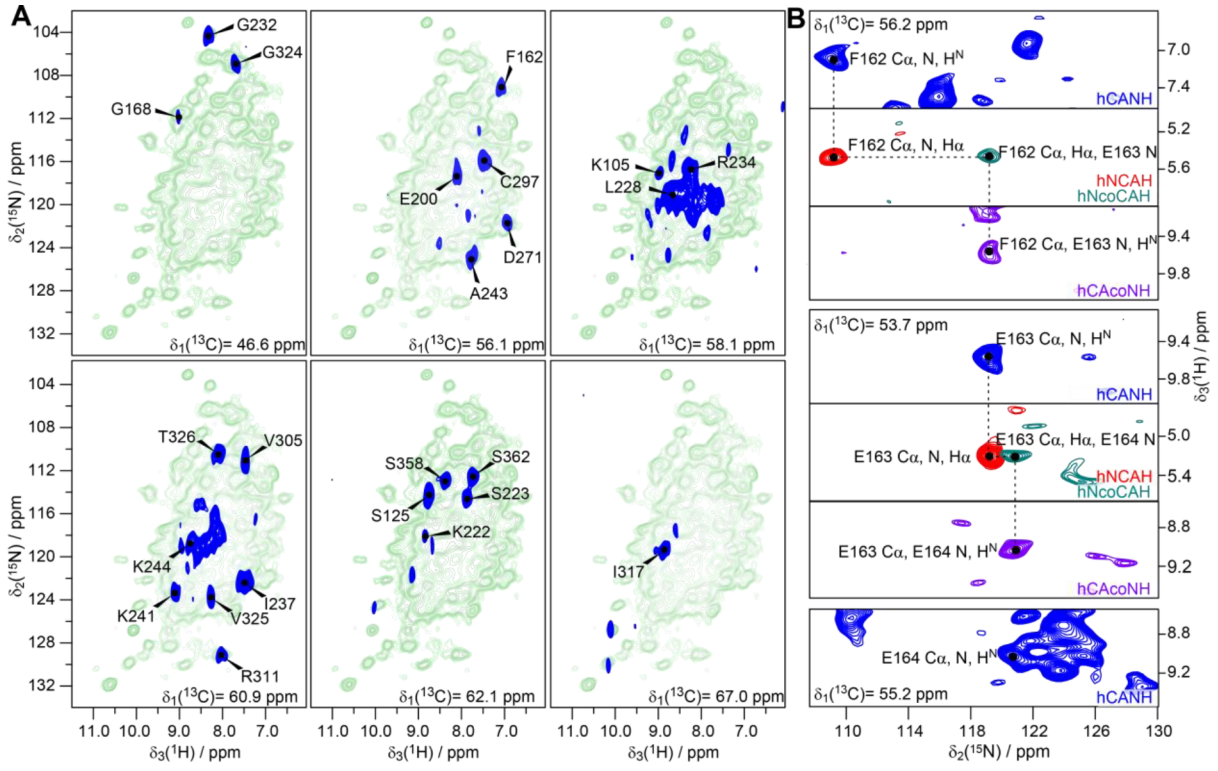

Figure 2. Protein resonance assignment by ^{1}H-detected solid-state NMR spectroscopy. (**A**) Representative 2D planes of 3D hCANH spectra (blue) and hNH spectrum (light green) of pRN1:ATP:DNA recorded at a MAS frequency of 100 kHz. (**B**) Strip plots illustrating the 3D sequential resonance assignment with four experiments: hCANH (blue), hNCAH (red), hNcoCAH (green), and hCAcoNH (purple).

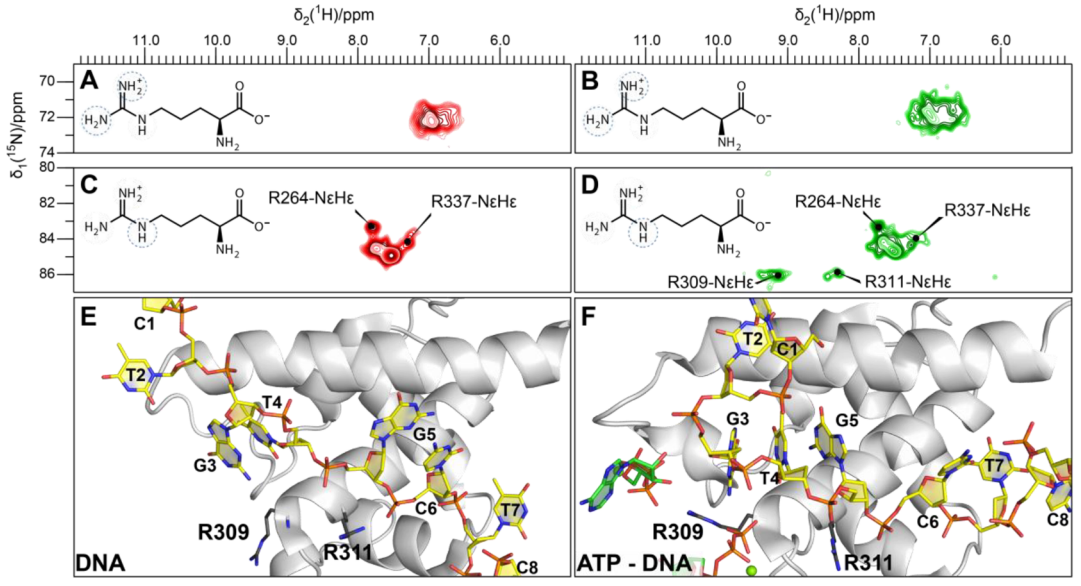

Figure 3. Arginine side-chains detected in solid-state NMR hNH spectra. Comparison of hNH spectra showing the arginine side-chain region for the pRN1:DNA (**A** Nη−Hη correlations and **C** Nε−Hε correlations) and pRN1:ATP:DNA complexes (**B** Nη−Hη correlations and **D** Nε−Hε correlations). Upon ATP-binding, R309 and R311 become detectable in the spectra, the first one at high proton chemical-shift values compatible with hydrogen-bond formation. Structures (**E** and **F**) are prepared from the PDB files 6GVU and 6GVT using pymol.[64] The carbon atoms of DNA and ATP are shown in yellow and green, respectively.

solid state. The averaged differences between solid- and solution-state chemical shifts (the latter for the HBD only) are determined to be 0.2 ppm for $^{1}H^{N}$, 0.1 ppm for $^{1}H^{A}$, 0.2 ppm for $^{13}C^{A}$, and 0.3 ppm for ^{15}N. Representative strip plots are shown in Figure 2B for the F162 to E164 stretch. Here, 160 out of 330 residues (~50%) of pRN1 and 45% of the Prim_Pol domain were assigned (BMRB accession code 50385). The solution-state NMR assignments used herein for the Prim_Pol domain will be described in a forthcoming publication.

Arginine and Lysine Side-Chains Detected by ^{1}H-Detected Spectroscopy at Fast MAS. Arginine and lysine side-chains are key elements participating in binding to

https://dx.doi.org/10.1021/acs.jpcb.0c08150
J. Phys. Chem. B 2020, 124, 11089−11097

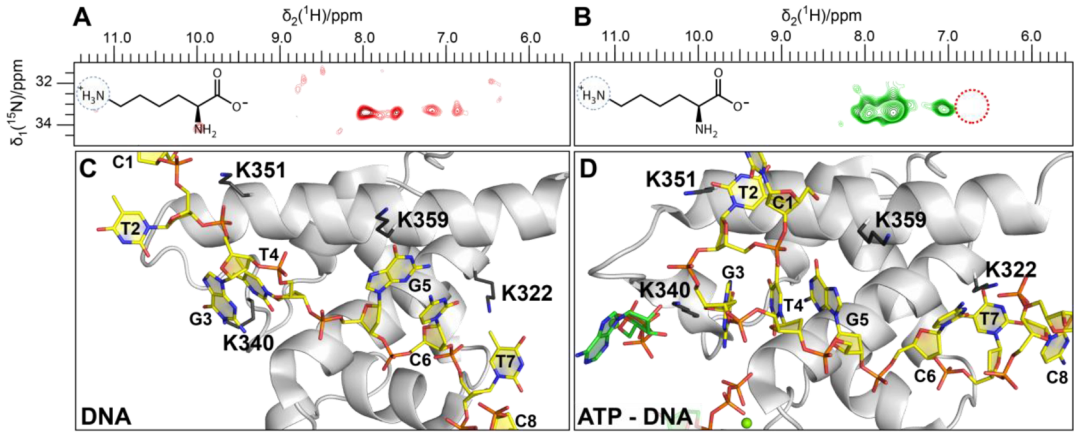

Figure 4. Lysine side-chains detected in solid-state NMR hNH spectra. Comparison of hNH spectra (**A** and **B**) showing the lysine side-chain region for the pRN1:DNA (**A**) and pRN1:ATP:DNA (**B**). Structures (**C** and **D**) are prepared from the PDB files 6GVU and 6GVT using pymol.[64] The red circle highlights a missing lysine correlation for the pRN1:ATP:DNA compared to the pRN1:DNA complex. The carbon atoms of DNA and ATP are shown in yellow and green, respectively.

nucleotides, either via hydrogen-bond formation or electrostatic interactions.[2] Figure 3 shows a selected region with arginine side-chain resonances from the hNH spectra of the samples with and without ATP. In pRN1:ATP:DNA (Figure 3B and D), two additional resonances are detected at high $^{15}N\varepsilon$ chemical-shift values compared to the binary complex (pRN1:DNA, Figure 3A and C). The proton with the most deshielded ^{1}H resonance (9.1 ppm) is assigned to R309 anchoring the bound ATP molecules in agreement with previous NMR studies in solution and in solid state (see also Figure 3E and F for a structural visualization).[58] The assignment is based on the ^{15}N chemical-shift value previously identified in NHHP solid-state NMR spectra.[58] The peak at lower ^{1}H chemical shift (8.3 ppm) corresponds to R311 coordinating the phosphate group of G5. Hydrogen bonding is encoded in the ^{1}H chemical-shift values:[23] R309 bridges two ATP molecules in the NMR-based structure and could hydrogen bond with one ATP Pγ atom. Solid-state NMR allows assignment of the Hε protons of the arginine guanidinium group confirming a similar deshielding effect observed for R309 in solution.[58] R311 Hε, only visible in the pRN1:ATP:DNA spectra, is not as strongly deshielded (8.3 ppm) but could potentially form a hydrogen-bond contact with the DNA oxygen-phosphate (G5), similar to the HBD:ATP:DNA complex (see also Figure 3F).[58] Both resonances are absent in the CP-based spectra of the binary complex, most likely because of side-chain flexibility. Previous results[58] showed that R311 does not stabilize the DNA in the binary complex and changes its conformation upon ATP and magnesium binding. The resolution of the hNH spectrum is however not sufficient to assign any arginine Hη1/Hη2 protons from the 2D spectrum, although their visibility indicates their rigidification upon DNA/ATP binding (Figure 3A and B).

Lysine side-chains have an important role in protein−DNA recognition, mainly by forming salt bridges with the negatively charged oxygen-phosphate groups.[3,65] The hNH spectra showing the lysine side-chain region are compared in Figure 4 for both complexes, pRN1:DNA and pRN1:ATP:DNA. Only rigidified lysine side-chains can be observed in such cross-polarization based spectra. While for the binary complex four resonances are detected (K322, K340, K351, and K359, Figure 4A), only three isolated resonances are found for pRN1:ATP:DNA (most likely K322, K340 and K351, Figure 4B). K359 binds to the DNA in pRN1:DNA and might be less crucial in pRN1:ATP:DNA (Figure 4 C and D). Unlike arginine side-chains where hydrogen bonding leads to characteristic ^{1}H chemical-shift values, proton chemical shifts of lysine side-chains involved in salt bridges are usually between 7 and 8 ppm.[26]

Aromatic ^{1}H-Resonances Detected with Solid State NMR. Aromatic residues also significantly contribute to the stability of nucleic acid−protein complexes. Indeed, tryptophan, tyrosine, and phenylalanine residues can potentially stabilize DNA bases through van-der-Waals interactions. Tryptophan and tyrosine side-chains can also be involved in hydrogen bonds.[2] In Figure 5, we show details of the aromatic region of a hCH correlation spectra recorded on the two complexes: pRN1:DNA (Figure 5A) and pRN1:DNA:ATP (Figure 5B). The assignments were transferred from solution-state NMR. Chemical shift perturbations (CSPs) upon ATP binding were detected (Figure 5C).

Figure 5D overlays the tryptophan side-chain region of the pRN1:DNA and pRN1:ATP:DNA hNH spectra. Characteristic CSPs upon ATP binding for HεNε resonances of Trp are labeled. In particular, the side-chain of W347 appears, upon ATP-binding, at a high ^{1}H chemical-shift value (10.8 ppm). This result is compatible with the formation of a hydrogen bond between W347 Hε and the oxygen-phosphate group of G3. This hypothesis is also supported by solution data (downfield shifted HεNε) and some atomic-scale models of the quaternary HBD complex (HBD:ATP:ATP:DNA).[58] We speculate that this hydrogen bond is favored in the pRN1 complex as shown by the solid-state NMR data. The W314 side-chain located in α-helix 10 is shifted upon ATP binding reflecting the stacking of G5 between W314 and T4. This is compatible with a DNA stabilization[58] (Figure 5E and F).

In ^{13}C-detected ^{15}N,^{13}C correlation experiments (MAS frequency 17 kHz) a selective CP step,[66] with the ^{13}C rf-carrier set to the aromatic region (~130 ppm), only tryptophan side-chain resonances are detected (Figure 6A). Most peaks in that spectrum were assigned thanks to the ^{15}N chemical shifts obtained from hNH correlation spectra (Figure 6C). Interestingly, W347 involved in DNA binding in pRN1:ATP:DNA remains rather weak in such a spectrum, in agreement with the hNH spectrum indicating some residual flexibility. However, no correlations for W347 were detected in pRN1:DNA underlining its intrinsic dynamics. Comparing the spectra of pRN1:DNA and pRN1:ATP:DNA, the tryptophans W72 of the Prim_Pol

https://dx.doi.org/10.1021/acs.jpcb.0c08150
J. Phys. Chem. B 2020, 124, 11089−11097

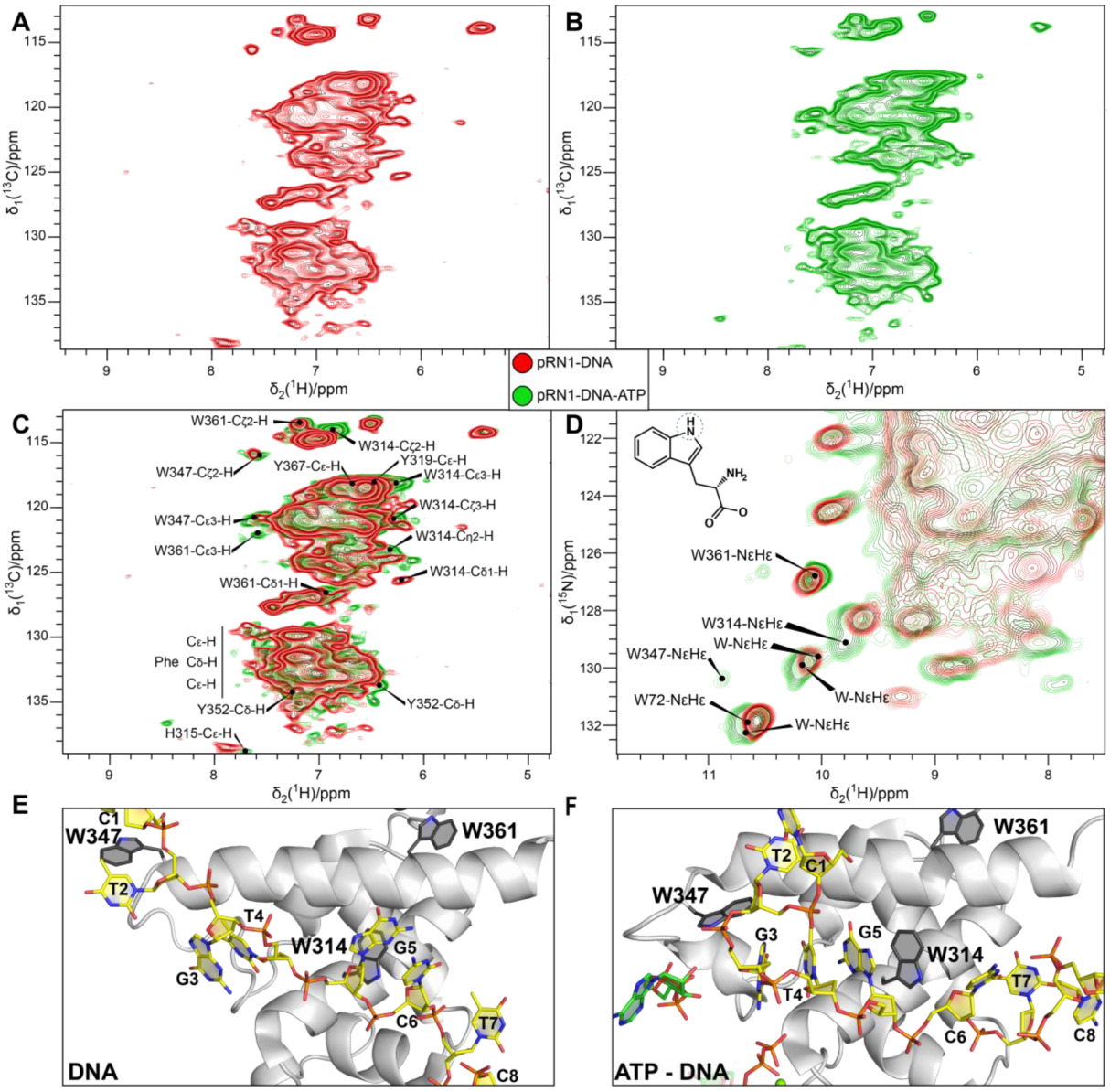

Figure 5. Aromatic side-chain region detected by ^{1}H fast MAS solid-state NMR. (**A**) hCH solid-state NMR spectrum of pRN1:DNA and (**B**) pRN1:ATP:DNA. (**C**) Overlay of the assigned spectra. (**D**) Superimposition of hNH spectra for the Trp side-chain region. The structures in **E** and **F** were drawn from the PDB files 6GVU and 6GVT using pymol.[64] Carbon atoms of DNA and ATP are shown in yellow and green, respectively.

and W361 of the HBD are slightly shifted in the ^{1}H dimension (Figure 6D). This might reveal the initiation of allosteric communications or a relative repositioning of the two domains upon ATP binding and is further supported by a couple of CSPs assigned to the Prim_Pol domain in the ^{13}C−^{13}C DARR spectra (see Figure S2). However, more investigations are required to detail domains rearrangements upon DNA binding with and without ATP in the interaction buffer.

A similar selective excitation approach for NC spin pairs was also applied in ^{1}H-detected experiments at 100 kHz MAS by adding an additional NC CP step within an hCH experiment (hnCH experiment, e.g., also described in ref 37 for applications on histidine side-chains; see Figures 1 and 6B and D). These spectra are rather sparse and allow the identification of Trp side-chains (Cδ1,Hδ1 or Cζ2,Hζ2 correlations). In the binary complex (Figure 6B) four resonances can be clearly identified in the spectrum. Using the assignment from the ^{15}N−^{1}H solution-state TROSY-HSQC, the solid-state hNH and SPECIFIC ^{15}N−^{13}C spectra, the resonances were assigned to Cδ1,Hδ1 side-chains of W361, W72 and an additional unassigned Trp of the Prim_Pol domain (W49, W121, W198, or W246). The W314 Cζ2,Hζ2 side-chain can also be observed with a high intensity. The comparison with pRN1:DNA shows that, in the presence of ATP, the spectrum is different (Figure 6D). Chemical-shift variations are found for W361 (Δ^{1}Hδ = 0.2 ppm) and W314 (Δ^{13}Cδ = 0.7 ppm), and the intensity of W314Cζ2,Hζ2 in the presence of ATP is strongly attenuated. This points to residual flexibility in the pRN1:ATP:DNA complex suggesting a putative sliding of the primase along the primer during polymerization.

CONCLUSIONS

We herein describe proton-detected solid-state NMR approaches at fast MAS frequencies to detect protein−DNA interactions in the 330 residues functional pRN1 primase by comparing pRN1:DNA complexes without and with ATP in

https://dx.doi.org/10.1021/acs.jpcb.0c08150
J. Phys. Chem. B 2020, 124, 11089−11097

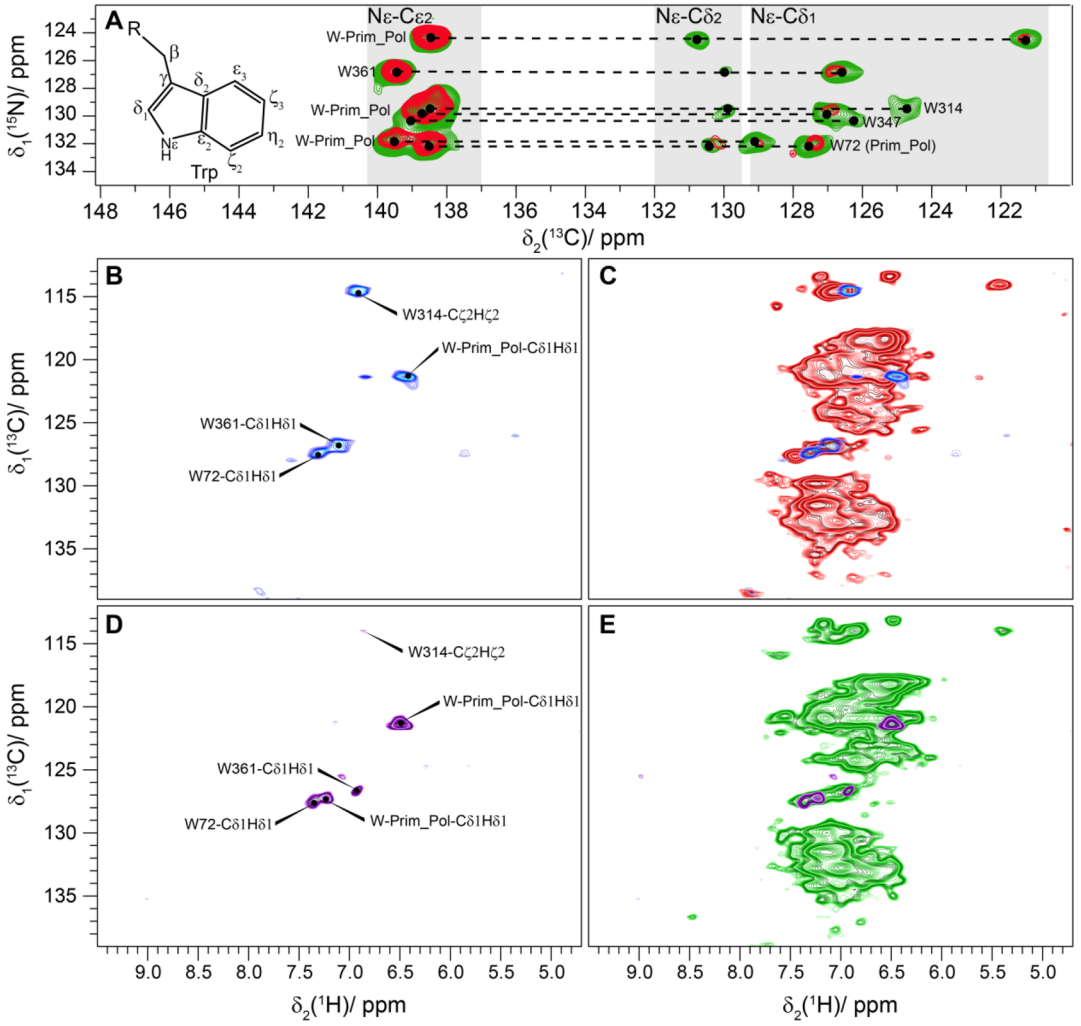

Figure 6. Solid-state NMR spectroscopic approaches to detect tryptophan side-chains. (**A**) SPECIFIC ^{15}N, ^{13}C spectra recorded at a MAS frequency of 17 kHz showing Trp side-chains for pRN1:DNA (shown in red) and pRN1:ATP:DNA (shown in green). Assignments are shown on the spectrum. (**B**) ^{13}C,^{1}H 2D hnCH spectrum recorded at a MAS frequency of 100 kHz of the binary complex selectively exciting only NC pairs of Trp side-chains (for the overlay with the hCH spectrum see part **C**). (**D**) ^{13}C,^{1}H 2D hnCH spectrum of pRN1:ATP:DNA selectively exciting only N−C pairs of Trp side-chains (for the overlay with the hCH spectrum see part **E**).

interaction buffer. Solid-state NMR allows probing these contacts in protein-nucleic acids complexes with multiple domains limiting the need of time-consuming modular approaches. The protein−ATP/DNA complexes studied by solid-state NMR are stable over time (the hydrolysis of ATP is significantly suppressed) and less than 1 mg of sample is needed for the experiments. ^{1}H-detected NMR spectra reveal key interactions mediated by lysine and arginine side-chains involved in noncovalent contacts with DNA or ATP, such as hydrogen bonds (manifested in the NMR spectra by high-frequency shifts) and salt bridges (observed in the spectra due to their rigidification upon DNA-binding). Aromatic side-chains are characterized in ^{13}C- and ^{1}H-detected spectra. The spectral overlap in such experiments is reduced by a selective excitation of NC spin pairs allowing us to selectively detect tryptophan side-chains and to identify those located at the protein−DNA binding interface. The proton assignments presented herein can be further employed in solid-state NMR studies to probe contacts between protein proton spins and phosphorus spins of the ATP or DNA to unravel nucleotide binding modes. Our strategy could be extended to solid-state and integrated studies of protein−nucleic acid recognition in many challenging biological complexes.

EXPERIMENTAL SECTION

Protein Expression and Purification. Expression and purification of the functional pRN1 primase containing the HBD and the Prim_Pol domain (residues 40−370) were already described.[67] Briefly, transformed *E. coli* BL21 (DE3) Codon+ were grown at 30 °C and induced with 1 mM IPTG at O.D. of 0.6. Cells were harvested and lysed by sonication in 25 mM sodium phosphate pH 7.0 and 0.1% (v/v) Triton X-100. After centrifugation (34 000*g*, 45 min) the extracts were loaded onto a Ni-NTA Agarose gravity column, which was equilibrated with 25 mM sodium phosphate pH 7.0, 300 mM NaCl, and 6 mM imidazole. The column was washed, and the protein eluted with 150 mM imidazole. The imidazole was removed, and buffer exchanged by gel-filtration. Peak fractions were pooled and concentrated between 0.5 and 1 mM.

Protein Complex Formation. The pRN1:DNA complex is an equimolar mix of 0.8 nM of the functional primase titrated with the CTGTGCTCA DNA template (Microsynth). For the pRN1:ATP:DNA complex formation, the ATP was added in

https://dx.doi.org/10.1021/acs.jpcb.0c08150
J. Phys. Chem. B 2020, 124, 11089−11097

excess. We used a 1:1:4 molar ratio for [pRN1]:[DNA]:[ATP]. All samples were prepared in NaH_2PO_4/Na_2HPO_4 25 mM pH 7.0, NaCl 50 mM and 10 mM $MgCl_2$.

Solid-State NMR Experiments. pRN1:ATP:DNA and pRN1:DNA were sedimented at 210 000*g* during 16 h in 0.7 mm and thin-walled 3.2 mm MAS NMR rotors using home-built filling tools.[68] $^{15}N-^{13}C$ and proton-detected experiments were acquired on a Bruker AVANCE III 850 MHz spectrometer using a 3.2 mm Bruker Biospin "E-free" and a 0.7 mm triple resonance MAS probe (Bruker Biospin) at MAS frequencies of 17.0 kHz and 100 kHz. Spectra were referenced to DSS (4,4-dimethyl-4-silapentane-1-sulfonic acid) as an internal reference. The sample temperature was set to 278 and 288 K for the experiments in 3.2 and 0.7 mm probes, respectively.[53] The 2D spectra were processed with the software TOPSPIN (version 3.5, Bruker Biospin) with a sine squared window function, using a sine bell shift of 3. All spectra were analyzed with CcpNmr.[69] For further experimental details see the Supporting Information.

■ ASSOCIATED CONTENT

Supporting Information

The Supporting Information is available free of charge at https://pubs.acs.org/doi/10.1021/acs.jpcb.0c08150.

2D hNH solid-state NMR spectra, 2D DARR spectrum, experimental solid-state NMR parameters (PDF)

■ AUTHOR INFORMATION

Corresponding Authors

Frédéric H.-T. Allain − *Institute of Molecular Biology and Biophysics and Institute of Biochemistry, ETH Zurich, 8093 Zurich, Switzerland*; Email: allain@bc.biol.ethz.ch

Beat H. Meier − *Physical Chemistry, ETH Zurich, 8093 Zurich, Switzerland*; Email: beme@ethz.ch

Thomas Wiegand − *Physical Chemistry, ETH Zurich, 8093 Zurich, Switzerland*; orcid.org/0000-0003-3655-6150; Email: thomas.wiegand@phys.chem.ethz.ch

Authors

Denis Lacabanne − *Physical Chemistry, ETH Zurich, 8093 Zurich, Switzerland*

Julien Boudet − *Institute of Molecular Biology and Biophysics, ETH Zurich, 8093 Zurich, Switzerland*

Alexander A. Malär − *Physical Chemistry, ETH Zurich, 8093 Zurich, Switzerland*

Pengzhi Wu − *Institute of Molecular Biology and Biophysics and Institute of Biochemistry, ETH Zurich, 8093 Zurich, Switzerland*

Riccardo Cadalbert − *Physical Chemistry, ETH Zurich, 8093 Zurich, Switzerland*

Loic Salmon − *Institute of Molecular Biology and Biophysics, ETH Zurich, 8093 Zurich, Switzerland*; orcid.org/0000-0002-0249-6279

Complete contact information is available at: https://pubs.acs.org/10.1021/acs.jpcb.0c08150

Author Contributions

J.B., P.W., and L.S. prepared the samples, RC supported with rotor filling. D.L., A.A.M., and T.W. performed the solid-state NMR experiments. D.L., J.B., F.H.T.A., B.H.M., and T.W. analyzed the data. All authors contributed to the writing of the manuscript. F.H.T.A., B.H.M., and T.W. designed and supervised the research.

Notes

The authors declare no competing financial interest.

■ ACKNOWLEDGMENTS

T.W. acknowledges support by the ETH Career SEED-69 16-1 and the ETH Research Grant ETH-43 17-2. L.S. acknowledges support from the European Union Horizon 2020 Research and Innovation Program under Marie Sklodowska-Curie grant agreement 707635. B.H.M. was supported by the Swiss National Science Foundation (Grant 200020_159707) and by the European Research Council (ERC) under the European Union's Horizon 2020 research and innovation program (grant agreement no. 741863, FASTER). F.H.T.A. acknowledges support from the SNF grants 310030_163345 and 310030_141160.

■ REFERENCES

(1) Kollman, P. A. Noncovalent interactions. *Acc. Chem. Res.* **1977**, *10* (10), 365−371.

(2) Lejeune, D.; Delsaux, N.; Charloteaux, B.; Thomas, A.; Brasseur, R. Protein−nucleic acid recognition: Statistical analysis of atomic interactions and influence of DNA structure. *Proteins: Struct., Funct., Genet.* **2005**, *61* (2), 258−271.

(3) Anderson, K. M.; Esadze, A.; Manoharan, M.; Brüschweiler, R.; Gorenstein, D. G.; Iwahara, J. Direct Observation of the Ion-Pair Dynamics at a Protein−DNA Interface by NMR Spectroscopy. *J. Am. Chem. Soc.* **2013**, *135* (9), 3613−3619.

(4) Kellie, J. L.; Wilson, K. A.; Wetmore, S. D. DNA−protein π-interactions in nature: abundance, structure, composition and strength of contacts between aromatic amino acids and DNA nucleobases or deoxyribose sugar. *Nucleic Acids Res.* **2014**, *42* (10), 6726−6741.

(5) Luscombe, N. M.; Laskowski, R. A.; Thornton, J. M. Amino acid-base interactions: a three-dimensional analysis of protein-DNA interactions at an atomic level. *Nucleic Acids Res.* **2001**, *29* (13), 2860−2874.

(6) Itsathitphaisarn, O.; Wing, R. A.; Eliason, W. K.; Wang, J.; Steitz, T. A. The Hexameric Helicase DnaB Adopts a Nonplanar Conformation during Translocation. *Cell* **2012**, *151* (2), 267−277.

(7) Arias-Palomo, E.; Puri, N.; O'Shea Murray, V. L.; Yan, Q.; Berger, J. M. Physical Basis for the Loading of a Bacterial Replicative Helicase onto DNA. *Mol. Cell* **2019**, *74* (1), 173−184.

(8) Sugita, Y.; Matsunami, H.; Kawaoka, Y.; Noda, T.; Wolf, M. Cryo-EM structure of the Ebola virus nucleoprotein−RNA complex at 3.6 Å resolution. *Nature* **2018**, *563* (7729), 137−140.

(9) Hofmann, S.; Januliene, D.; Mehdipour, A. R.; Thomas, C.; Stefan, E.; Brüchert, S.; Kuhn, B. T.; Geertsma, E. R.; Hummer, G.; Tampé, R.; et al. Conformation space of a heterodimeric ABC exporter under turnover conditions. *Nature* **2019**, *571* (7766), 580−583.

(10) Soczek, K. M.; Grant, T.; Rosenthal, P. B.; Mondragón, A. CryoEM structures of open dimers of gyrase A in complex with DNA illuminate mechanism of strand passage. *eLife* **2018**, *7*, e41215.

(11) Glaeser, R. M. How good can cryo-EM become? *Nat. Methods* **2016**, *13* (1), 28−32.

(12) Tan, Y. Z.; Baldwin, P. R.; Davis, J. H.; Williamson, J. R.; Potter, C. S.; Carragher, B.; Lyumkis, D. Addressing preferred specimen orientation in single-particle cryo-EM through tilting. *Nat. Methods* **2017**, *14* (8), 793−796.

(13) Lyumkis, D. Challenges and opportunities in cryo-EM single-particle analysis. *J. Biol. Chem.* **2019**, *294* (13), 5181−5197.

(14) Dominguez, C.; Schubert, M.; Duss, O.; Ravindranathan, S.; Allain, F. H. T. Structure determination and dynamics of protein−RNA complexes by NMR spectroscopy. *Prog. Nucl. Magn. Reson. Spectrosc.* **2011**, *58* (1−2), 1−61.

(15) Campagne, S.; Gervais, V.; Milon, A. Nuclear magnetic resonance analysis of protein-DNA interactions. *J. R. Soc., Interface* **2011**, *8* (61), 1065−1078.

(16) Asami, S.; Rakwalska-Bange, M.; Carlomagno, T.; Reif, B. Protein−RNA Interfaces Probed by 1H-Detected MAS Solid-State NMR Spectroscopy. *Angew. Chem., Int. Ed.* **2013**, *52* (8), 2345−2349.
(17) Jehle, S.; Falb, M.; Kirkpatrick, J. P.; Oschkinat, H.; van Rossum, B.-J.; Althoff, G.; Carlomagno, T. Intermolecular Protein-RNA Interactions Revealed by 2D 31P-15N Magic Angle Spinning Solid-State NMR Spectroscopy. *J. Am. Chem. Soc.* **2010**, *132* (11), 3842−3846.
(18) Huang, W.; Varani, G.; Drobny, G. P. Interactions of protein side chains with RNA defined with REDOR solid state NMR. *J. Biomol. NMR* **2011**, *51* (3), 347.
(19) Huang, W.; Varani, G.; Drobny, G. P. 13C/15N−19F Intermolecular REDOR NMR Study of the Interaction of TAR RNA with Tat Peptides. *J. Am. Chem. Soc.* **2010**, *132* (50), 17643−17645.
(20) Morag, O.; Abramov, G.; Goldbourt, A. Complete Chemical Shift Assignment of the ssDNA in the Filamentous Bacteriophage fd Reports on Its Conformation and on Its Interface with the Capsid Shell. *J. Am. Chem. Soc.* **2014**, *136* (6), 2292−2301.
(21) Ahmed, M.; Marchanka, A.; Carlomagno, T. Structure of a Protein-RNA Complex by Solid-State NMR Spectroscopy. *Angew. Chem., Int. Ed.* **2020**, *59* (17), 6866−6873.
(22) Wiegand, T. A solid-state NMR tool box for the investigation of ATP-fueled protein engines. *Prog. Nucl. Magn. Reson. Spectrosc.* **2020**, *117*, 1−32.
(23) Wagner, G.; Pardi, A.; Wuethrich, K. Hydrogen bond length and proton NMR chemical shifts in proteins. *J. Am. Chem. Soc.* **1983**, *105* (18), 5948−5949.
(24) Wiegand, T.; Schledorn, M.; Malär, A. A.; Cadalbert, R.; Däpp, A.; Terradot, L.; Meier, B. H.; Böckmann, A. Nucleotide binding modes in a motor protein revealed by ^{31}P- and ^{1}H-detected MAS solid-state NMR. *ChemBioChem* **2020**, *21*, 324−330.
(25) Baird-Titus, J. M.; Thapa, M.; Doerdelmann, T.; Combs, K. A.; Rance, M. Lysine Side-Chain Dynamics in the Binding Site of Homeodomain/DNA Complexes As Observed by NMR Relaxation Experiments and Molecular Dynamics Simulations. *Biochemistry* **2018**, *57* (19), 2796−2813.
(26) Wiegand, T.; Cadalbert, R.; Lacabanne, D.; Timmins, J.; Terradot, L.; Bockmann, A.; Meier, B. H. The conformational changes coupling ATP hydrolysis and translocation in a bacterial DnaB helicase. *Nat. Commun.* **2019**, *10* (1), 31.
(27) Gath, J.; Bousset, L.; Habenstein, B.; Melki, R.; Böckmann, A.; Meier, B. H. Unlike Twins: An NMR Comparison of Two α-Synuclein Polymorphs Featuring Different Toxicity. *PLoS One* **2014**, *9* (3), e90659.
(28) Schlundt, A.; Tants, J.-N.; Sattler, M. Integrated structural biology to unravel molecular mechanisms of protein-RNA recognition. *Methods* **2017**, *118−119*, 119−136.
(29) Kay, L. E. Solution NMR spectroscopy of supra-molecular systems, why bother? A methyl-TROSY view. *J. Magn. Reson.* **2011**, *210* (2), 159−170.
(30) Lacabanne, D.; Meier, B. H.; Bockmann, A. Selective labeling and unlabeling strategies in protein solid-state NMR spectroscopy. *J. Biomol. NMR* **2018**, *71* (3), 141−150.
(31) Mas, G.; Crublet, E.; Hamelin, O.; Gans, P.; Boisbouvier, J. Specific labeling and assignment strategies of valine methyl groups for NMR studies of high molecular weight proteins. *J. Biomol. NMR* **2013**, *57* (3), 251−262.
(32) Mas, G.; Guan, J.-Y.; Crublet, E.; Debled, E. C.; Moriscot, C.; Gans, P.; Schoehn, G.; Macek, P.; Schanda, P.; Boisbouvier, J. Structural investigation of a chaperonin in action reveals how nucleotide binding regulates the functional cycle. *Science Advances* **2018**, *4* (9), eaau4196.
(33) Andreas, L. B.; Jaudzems, K.; Stanek, J.; Lalli, D.; Bertarello, A.; Le Marchand, T.; Cala-De Paepe, D.; Kotelovica, S.; Akopjana, I.; Knott, B.; et al. Structure of fully protonated proteins by proton-detected magic-angle spinning NMR. *Proc. Natl. Acad. Sci. U. S. A.* **2016**, *113* (33), 9187−9192.
(34) Agarwal, V.; Penzel, S.; Szekely, K.; Cadalbert, R.; Testori, E.; Oss, A.; Past, J.; Samoson, A.; Ernst, M.; Böckmann, A.; et al. De Novo 3D Structure Determination from Sub-milligram Protein Samples by Solid-State 100 kHz MAS NMR Spectroscopy. *Angew. Chem., Int. Ed.* **2014**, *53* (45), 12253−12256.
(35) Stöppler, D.; Macpherson, A.; Smith-Penzel, S.; Basse, N.; Lecomte, F.; Deboves, H.; Taylor, R. D.; Norman, T.; Porter, J.; Waters, L. C.; et al. Insight into small molecule binding to the neonatal Fc receptor by X-ray crystallography and 100 kHz magic-angle-spinning NMR. *PLoS Biol.* **2018**, *16* (5), No. e2006192.
(36) Medeiros-Silva, J.; Jekhmane, S.; Paioni, A. L.; Gawarecka, K.; Baldus, M.; Swiezewska, E.; Breukink, E.; Weingarth, M. High-resolution NMR studies of antibiotics in cellular membranes. *Nat. Commun.* **2018**, *9* (1), 3963.
(37) Vasa, S. K.; Singh, H.; Grohe, K.; Linser, R. Assessment of a Large Enzyme-Drug Complex by Proton-Detected Solid-State NMR Spectroscopy without Deuteration. *Angew. Chem., Int. Ed.* **2019**, *58* (17), 5758−5762.
(38) Stanek, J.; Andreas, L. B.; Jaudzems, K.; Cala, D.; Lalli, D.; Bertarello, A.; Schubeis, T.; Akopjana, I.; Kotelovica, S.; Tars, K.; et al. NMR Spectroscopic Assignment of Backbone and Side-Chain Protons in Fully Protonated Proteins: Microcrystals, Sedimented Assemblies, and Amyloid Fibrils. *Angew. Chem., Int. Ed.* **2016**, *55* (50), 15504−15509.
(39) Nishiyama, Y.; Malon, M.; Ishii, Y.; Ramamoorthy, A. 3D 15N/15N/1H chemical shift correlation experiment utilizing an RFDR-based 1H/1H mixing period at 100kHz MAS. *J. Magn. Reson.* **2014**, *244*, 1−5.
(40) Struppe, J.; Quinn, C. M.; Lu, M.; Wang, M.; Hou, G.; Lu, X.; Kraus, J.; Andreas, L. B.; Stanek, J.; Lalli, D.; et al. Expanding the horizons for structural analysis of fully protonated protein assemblies by NMR spectroscopy at MAS frequencies above 100 kHz. *Solid State Nucl. Magn. Reson.* **2017**, *87*, 117−125.
(41) Schubeis, T.; Le Marchand, T.; Andreas, L. B.; Pintacuda, G. 1H magic-angle spinning NMR evolves as a powerful new tool for membrane proteins. *J. Magn. Reson.* **2018**, *287*, 140−152.
(42) Vasa, S. K.; Rovó, P.; Linser, R. Protons as Versatile Reporters in Solid-State NMR Spectroscopy. *Acc. Chem. Res.* **2018**, *51* (6), 1386−1395.
(43) Barbet-Massin, E.; Pell, A. J.; Retel, J. S.; Andreas, L. B.; Jaudzems, K.; Franks, W. T.; Nieuwkoop, A. J.; Hiller, M.; Higman, V.; Guerry, P.; et al. Rapid Proton-Detected NMR Assignment for Proteins with Fast Magic Angle Spinning. *J. Am. Chem. Soc.* **2014**, *136* (35), 12489−12497.
(44) Xue, K.; Sarkar, R.; Tosner, Z.; Lalli, D.; Motz, C.; Koch, B.; Pintacuda, G.; Reif, B. MAS dependent sensitivity of different isotopomers in selectively methyl protonated protein samples in solid state NMR. *J. Biomol. NMR* **2019**, *73* (10), 625−631.
(45) Marchanka, A.; Stanek, J.; Pintacuda, G.; Carlomagno, T. Rapid access to RNA resonances by proton-detected solid-state NMR at > 100 kHz MAS. *Chem. Commun. (Cambridge, U. K.)* **2018**, *54* (65), 8972−8975.
(46) Gardiennet, C.; Schütz, A. K.; Hunkeler, A.; Kunert, B.; Terradot, L.; Böckmann, A.; Meier, B. H. A Sedimented Sample of a 59 kDa Dodecameric Helicase Yields High-Resolution Solid-State NMR Spectra. *Angew. Chem., Int. Ed.* **2012**, *51* (31), 7855−7858.
(47) Bertini, I.; Luchinat, C.; Parigi, G.; Ravera, E.; Reif, B.; Turano, P. Solid-state NMR of proteins sedimented by ultracentrifugation. *Proc. Natl. Acad. Sci. U. S. A.* **2011**, *108* (26), 10396−10399.
(48) Wiegand, T.; Lacabanne, D.; Torosyan, A.; Boudet, J.; Cadalbert, R.; Allain, F. H.; Meier, B. H.; Bockmann, A. Sedimentation Yields Long-Term Stable Protein Samples as Shown by Solid-State NMR. *Front Mol. Biosci* **2020**, *7* (17), 17.
(49) Carlomagno, T. Present and future of NMR for RNA−protein complexes: A perspective of integrated structural biology. *J. Magn. Reson.* **2014**, *241*, 126−136.
(50) Blanco, F. J.; Montoya, G. Transient DNA/RNA-protein interactions. *FEBS J.* **2011**, *278* (10), 1643−1650.
(51) Wiegand, T.; Cadalbert, R.; von Schroetter, C.; Allain, F. H.-T.; Meier, B. H. Segmental isotope labelling and solid-state NMR of a 12 × 59 kDa motor protein: identification of structural variability. *J. Biomol. NMR* **2018**, *71*, 237−245.

https://dx.doi.org/10.1021/acs.jpcb.0c08150
J. Phys. Chem. B 2020, 124, 11089−11097

(52) Frederick, K. K.; Michaelis, V. K.; Caporini, M. A.; Andreas, L. B.; Debelouchina, G. T.; Griffin, R. G.; Lindquist, S. Combining DNP NMR with segmental and specific labeling to study a yeast prion protein strain that is not parallel in-register. *Proc. Natl. Acad. Sci. U. S. A.* **2017**, *114* (14), 3642−3647.
(53) Schubeis, T.; Lührs, T.; Ritter, C. Unambiguous Assignment of Short- and Long-Range Structural Restraints by Solid-State NMR Spectroscopy with Segmental Isotope Labeling. *ChemBioChem* **2015**, *16* (1), 51−54.
(54) Beck, K.; Lipps, G. Properties of an unusual DNA primase from an archaeal plasmid. *Nucleic Acids Res.* **2007**, *35* (17), 5635−5645.
(55) Frick, D. N.; Richardson, C. C. DNA Primases. *Annu. Rev. Biochem.* **2001**, *70* (1), 39−80.
(56) Beck, K.; Vannini, A.; Cramer, P.; Lipps, G. The archaeo-eukaryotic primase of plasmid pRN1 requires a helix bundle domain for faithful primer synthesis. *Nucleic Acids Res.* **2010**, *38* (19), 6707−6718.
(57) Boudet, J.; Devillier, J.-C.; Allain, F. H. T.; Lipps, G. Structures to complement the archaeo-eukaryotic primases catalytic cycle description: What's next? *Comput. Struct. Biotechnol. J.* **2015**, *13*, 339−351.
(58) Boudet, J.; Devillier, J.-C.; Wiegand, T.; Salmon, L.; Meier, B. H.; Lipps, G.; Allain, F. H.-T. A Small Helical Bundle Prepares Primer Synthesis by Binding Two Nucleotides that Enhance Sequence-Specific Recognition of the DNA Template. *Cell* **2019**, *176* (1−2), 154−166.
(59) Lipps, G. Structure and function of the primase domain of the replication protein from the archaeal plasmid pRN1. *Biochem. Soc. Trans.* **2011**, *39* (1), 104−106.
(60) Sternberg, U.; Witter, R.; Kuprov, I.; Lamley, J. M.; Oss, A.; Lewandowski, J. R.; Samoson, A. 1H line width dependence on MAS speed in solid state NMR − Comparison of experiment and simulation. *J. Magn. Reson.* **2018**, *291*, 32−39.
(61) Cala-De Paepe, D.; Stanek, J.; Jaudzems, K.; Tars, K.; Andreas, L. B.; Pintacuda, G. Is protein deuteration beneficial for proton detected solid-state NMR at and above 100 kHz magic-angle spinning? *Solid State Nucl. Magn. Reson.* **2017**, *87*, 126−136.
(62) Penzel, S.; Oss, A.; Org, M. L.; Samoson, A.; Bockmann, A.; Ernst, M.; Meier, B. H. Spinning faster: protein NMR at MAS frequencies up to 126 kHz. *J. Biomol. NMR* **2019**, *73* (1−2), 19−29.
(63) Schledorn, M.; Malar, A. A.; Torosyan, A.; Penzel, S.; Klose, D.; Oss, A.; Org, M. L.; Wang, S.; Lecoq, L.; Cadalbert, R.; et al. Protein NMR Spectroscopy at 150 kHz Magic-Angle Spinning Continues To Improve Resolution and Mass Sensitivity. *ChemBioChem* **2020**, *21* (17), 2540−2548.
(64) The PyMOL Molecular Graphics System, V.S., LLC.
(65) Esadze, A.; Li, D.-W.; Wang, T.; Brüschweiler, R.; Iwahara, J. Dynamics of Lysine Side-Chain Amino Groups in a Protein Studied by Heteronuclear 1H−15N NMR Spectroscopy. *J. Am. Chem. Soc.* **2011**, *133* (4), 909−919.
(66) Baldus, M.; Petkova, A. T.; Herzfeld, J.; Griffin, R. G. Cross polarization in the tilted frame: assignment and spectral simplification in heteronuclear spin systems. *Mol. Phys.* **1998**, *95* (6), 1197−1207.
(67) Lipps, G.; Röther, S.; Hart, C.; Krauss, G. A novel type of replicative enzyme harbouring ATPase, primase and DNA polymerase activity. *EMBO J.* **2003**, *22* (10), 2516−2525.
(68) Böckmann, A.; Gardiennet, C.; Verel, R.; Hunkeler, A.; Loquet, A.; Pintacuda, G.; Emsley, L.; Meier, B.; Lesage, A. Characterization of different water pools in solid-state NMR protein samples. *J. Biomol. NMR* **2009**, *45* (3), 319−327.
(69) Vranken, W. F.; Boucher, W.; Stevens, T. J.; Fogh, R. H.; Pajon, A.; Llinas, M.; Ulrich, E. L.; Markley, J. L.; Ionides, J.; Laue, E. D. The CCPN data model for NMR spectroscopy: Development of a software pipeline. *Proteins: Struct., Funct., Genet.* **2005**, *59* (4), 687−696.

https://dx.doi.org/10.1021/acs.jpcb.0c08150
J. Phys. Chem. B 2020, 124, 11089−11097